TURBULENT PARAMETERS AT DIFFERENT HEIGHTS IN THE ATMOSPHERE. SHACK—HARTMANN WAVEFRONT SENSOR DATA

A.Yu. Shikhovtsev (iD)
*Institute of Solar-Terrestrial Physics SB RAS,
Irkutsk, Russia, artempochta2009@rambler.ru*

A.V. Kiselev (iD)
*Institute of Solar-Terrestrial Physics SB RAS,
Irkutsk, Russia, kiselev@iszf.irk.ru*

P.G. Kovadlo (iD)
*Institute of Solar-Terrestrial Physics SB RAS,
Irkutsk, Russia, kovadlo2006@rambler.ru*

D.Yu. Kolobov (iD)
*Institute of Solar-Terrestrial Physics SB RAS,
Irkutsk, Russia, kolobov@iszf.irk.ru*

I.V. Russkikh (iD)
*Institute of Solar-Terrestrial Physics SB RAS,
Irkutsk, Russia, vanekrus@iszf.irk.ru*

V.E. Tomin
*Institute of Solar-Terrestrial Physics SB RAS,
Irkutsk, Russia, tomin@iszf.irk.ru*

Abstract. The paper presents the results of studies of wavefront distortions at different heights in the atmosphere. We have used measurement wavefront data to determine optical turbulence parameters along the line of sight of the Large Solar Vacuum Telescope. Through cross-correlation analysis of differential motions of sunspots at spaced wavefront sensor subapertures, we determined turbulent parameters at different heights at the Large Solar Vacuum Telescope site. The differential motions of sunspots characterize the small-scale structure of turbulent phase distortions in the atmosphere. Synchronous temporal changes in the amplitude of these distortions at certain regions of the telescope aperture are conditioned by turbulent layers at different heights. We have estimated the contribution of optical turbulence to integral distortions at the telescope aperture for layers 0–0.6, 0.6–1.1, 1.1–1.7 km. The contribution of optical turbulence concentrated in a 1.7 km atmospheric layer to the wavefront distortions at the aperture telescope is shown to be ~43 %.

Keywords: telescope, wavefront, turbulence profiles, adaptive optics.

INTRODUCTION

Designing and refining the technical characteristics of both a classical adaptive optics (AO) system and an AO multisystem require information on the turbulence structure in the atmospheric boundary layer and free atmosphere [Bolbasova et al., 2021; Kleymenov et al., 2021; Rasouli et al., 2009; Rasouli, Rajabi, 2016]. In particular, it is necessary to know vertical profiles of the structure characteristic of air refractive index fluctuations C_n^2 and wind speed V. On the one hand, the vertical profiles C_n^2 and V determine the dynamic range of the AO system. On the other hand, the choice of parameters for deformable mirrors and Shack–Hartmann wavefront sensors in the classical AO system depends on the Fried parameter determined by the development of optical turbulence along the telescope line of sight. Classical adaptive systems are based on separate correction of wavefront slopes (tip/tilt aberrations) and aberrations of higher orders. The field of view in which the correction leads to a significant increase in the Strehl parameter is narrow and limited by the so-called isoplanatic angle of the atmosphere. At the Sayan Solar Observatory site, the characteristic values of the isoplanatic angle in the optical range of the electromagnetic spectrum are quite small, ranging from 1 to 3 arcsec. The isoplanatic angle changes mainly under the influence of the upper atmospheric layers, its statistically averaged value for the Sayan Solar Observatory is close to the statistically averaged value for the Baikal Astrophysical Observatory [Kovadlo et al., 2019].

The size of the field of view, within which high values of the Strehl parameter are observed, depends on the nature of optical turbulence distribution along the telescope line of sight and varies significantly with time. In this case, the turbulence of upper atmospheric layers, whose intensity may be high, makes the greatest contribution to a decrease in the size of the field of view. Modern AO systems that determine and correct wavefront distortions in a wide field of view include several wavefront sensors used to reconstruct vertical profiles of optical turbulence.

The problem of determining the vertical profiles of daytime optical turbulence should be solved to ensure the operation of AO systems with a wide field of view of an arbitrary large-aperture solar telescope. In particular, considerable attention is paid to measurements of vertical profiles of optical turbulence for the AO system of the European Solar Telescope (EST). Marco de la Rosa et al. [2016] have examined Strehl parameter variations across the telescope field of view as a function of the solar zenith angle, Fried parameter, and fraction of optical turbulence energy in the lower atmosphere. The variations were estimated for a field of view of ~1 arcmin. At a 10 cm Fried parameter, a 70° zenith angle, and 80 % optical turbulence energy in the lower atmos-

phere, the use of an additional deformable mirror is shown to lead to a significant increase in the Strehl parameter across the field of view (approximately 1.7 times). Conversely, at a zenith angle of 10°, the use of an additional deformable mirror leads to a decrease in the Strehl parameter across the field of view. Marco de la Rosa et al. [2016] show spatial distributions of the Strehl parameter for different atmospheric conditions and designs of AO systems. For correct comparison of the efficiency of AO system designs, we present the calculated data in a modified coordinate system averaged Strehl parameter — the number of the region separately for the periphery and for the central region of the field of view in systems with three and four deformable mirrors. This allows us to estimate the amplitudes of Strehl parameter variations. Strehl parameter variations across the field of view of a large-aperture telescope in an adaptive system with three and four deformable mirrors are depicted in Figure 1. Along the Y-axis are Strehl parameter values; along the X-axis is the region number. Distances between the regions whose positions correspond to certain areas at the telescope aperture are ~7 arcsec.

Analysis of Figure 1 shows that the amplitude of the Strehl parameter variations in the center of the field of view (lines 3 and 4) is much lower than that on its periphery. Such a pattern of changes in image quality characteristics is consistent with our calculations [Shikhovtsev et al., 2020; Shikhovtsev et al., 2021a; 2021b]. The Strehl parameter on the periphery and in the center of the field of view after wavefront correction depends not only on the number of deformable mirrors, but also on the vertical profile of the structure constant of turbulent air refractive index fluctuations. The largest Strehl parameter is achieved under light turbulence in the upper layers of the optically active atmosphere when the effective height of the turbulent atmosphere is small.

Thus, optimization of technical characteristics of AO systems requires information about vertical profiles of optical turbulence.
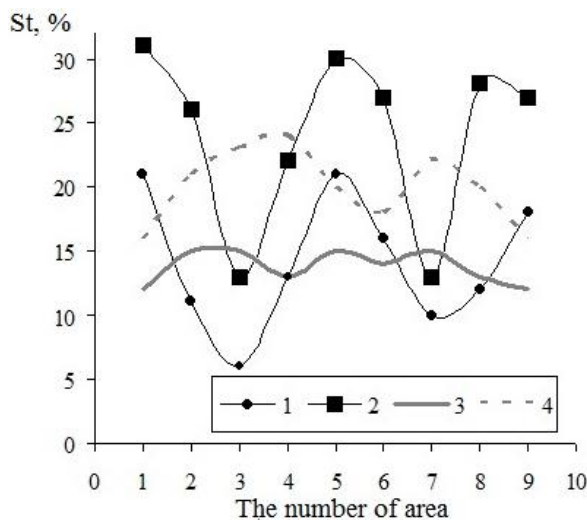

Figure 1. Strehl parameter variations across the telescope field of view. In the system with three and four deformable mirrors, lines 1 and 2 show Strehl parameter variations on the periphery of the field of view; lines 3 and 4, those in the center of the field of view. The dependencies are obtained from the data presented in [Marco de la Rosa et al., 2016]

METHOD OF MEASUREMENTS OF WAVEFRONT DISTORTIONS FORMED IN TURBULENT LAYERS AT DIFFERENT HEIGHTS

Considerable attention is paid to measurements of turbulent characteristics in the atmospheric boundary layer and overlying atmosphere in terms of determining the structure of atmospheric flows and the small-scale turbulence [Kornilov et al., 2009; Nosov et al., 2017; Banakh et al., 2021; Odintsov et al., 2019; Kamardin, Odintsov, 2017; Potekaev et al., 2021; Song et al., 2020].

We have used observational data from the Large Solar Vacuum Telescope (LSVT) of the Baikal Astrophysical Observatory with a primary mirror 1 m in diameter. The telescope is located in the village of Listvyanka close to the shoreline of Lake Baikal on one of the isolated peaks 210 m high above the lake surface. LSVT is equipped with a mock-up of AO system. Using the experimental base of LSVT, methods and approaches have been developed for reconstructing wavefront distortions [Botygina et al., 2018; Lavrinov, Lavrinova, 2019].

To determine the microstructure characteristics of turbulent layers, we have adopted the S-DIMM+ method [Wang et al., 2018] based on processing the measurement data obtained by the Shack—Hartmann wavefront sensor. In the summer experiments of 2020, LSVT made observations of sunspot center-of-gravity shifts in focal planes of the Shack–Hartmann wavefront sensor installed in the LSVT multicascade AO system [Lukin et al., 2019]. The measurements were made using the Shack–Hartmann wavefront sensor with a number of subapertures of 6×6 at 60 cm aperture of the telescope with a diaphragm. The sensor operation frequency was 100 Hz, the length in time realizations was ~30 000 frames. The August 11, 2020 observations provided time series of hartmannograms of two sunspots (Figure 2).

For each subaperture of the wavefront sensor, we assessed center-of-gravity shifts x, y in subimages of each sunspot. To estimate positions of peaks, we used the method of weighted centers of gravity [Kazakov et al., 2018; Lavrinov, Lavrinova, 2019]. Fragments of time realizations of the center-of-gravity shifts in sunspot subimages in the focal plane of the LSVT Shack—Hartmann wavefront sensor are presented in Figure 3.

Pearson's linear correlation coefficient between the center-of-gravity shifts in the subimages of two sunspots at spaced subapertures is high and amounts to 0.93. We use the time realizations of the center-of-gravity shifts in subimages of two sunspots to determine turbulence characteristics at different heights in the atmosphere.

In this work, to identify turbulent layers, we employ the relationship between the spatial cross-correlation function of differential center-of-gravity shifts in subimages and the vertical distribution of the structure constant of turbulent air refractive index fluctuations.

In the S-DIMM+ method, the center-of-gravity shifts in subimages along mutually perpendicular coordinate axes are proportional to the total contribution of different atmospheric layers:
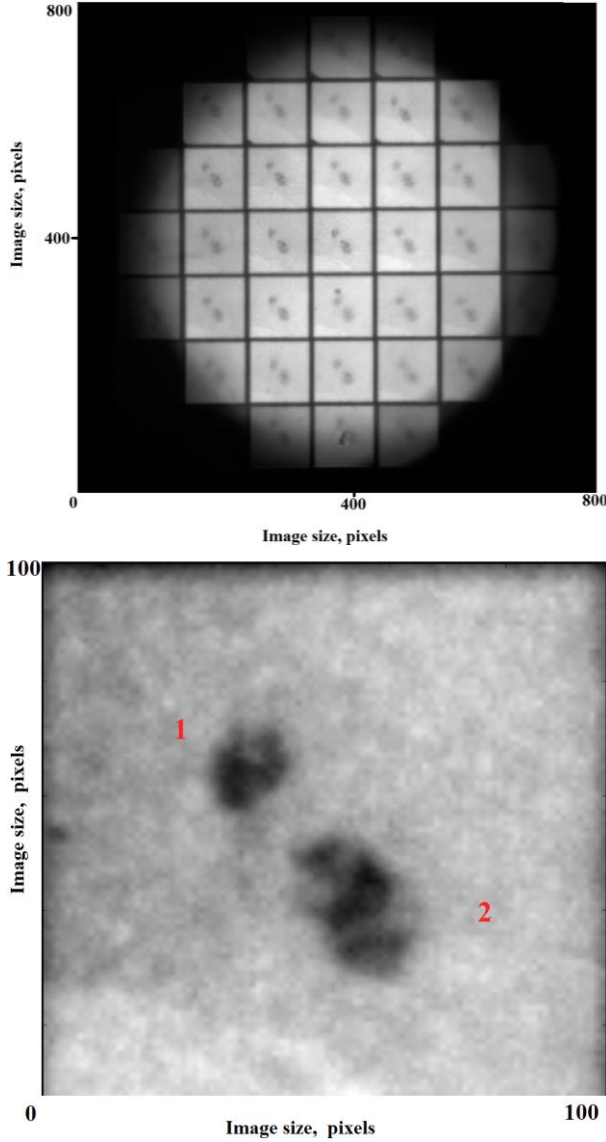
Figure 3. Fragments of time realizations of center-of-gravity shifts in sunspot subimages in the focal plane of the Shack–Hartmann wavefront sensor. Line 1 indicates center-of-gravity shifts in the subimage of the first sunspot in the reference subaperture of the wavefront sensor; line 2 shows center-of-gravity shifts in the subimage of the second sunspot in the wavefront sensor's subaperture offset by 6 cm

Using expressions (1) and (2), we can determine vertical profiles of structure parameters of atmospheric turbulence and wavefront distortions by analyzing the cross-correlation functions C_{sx} and C_{sy}, calculated from measurements made with the Shack-Hartmann wavefront sensor. The differential motions of sunspot centers along the X-axis are found as follows:

$$\delta x_1(s,0) = \sum_{n=1}^{N} \left\{ x_n(s) - x_n(0) \right\}, \tag{3}$$

$$\delta x_2(s,\alpha) = \sum_{n=1}^{N} \left\{ x_n(s + \alpha h_n) - x_n(\alpha h_n) \right\}, \tag{4}$$

where h_n is the position of the center of gravity of a sunspot.

The coefficients c_n are proportional to the intensity of optical turbulence in the atmospheric layer dh_n thick:

$$c_n = 5.98 D_{\text{eff}}^{-1/3}(h_n) C_n^2(h_n) dh_n / \cos\gamma, \tag{5}$$

where D_{eff} is the effective diameter of the telescope; γ is the zenith angle.

OPTICAL TURBULENCE AT DIFFERENT HEIGHTS IN THE ATMOSPHERE AT THE LARGE SOLAR VACUUM TELESCOPE SITE

To determine optical turbulence characteristics at different heights in the atmosphere, we have calculated spatial cross-correlation functions of differential center-of-gravity shifts of two sunspots at spaced subapertures of the Shack–Hartmann wavefront sensor.

Figure 2. Sunspot hartmannogram obtained in the AO system of the Large Solar Vacuum Telescope on August 11, 2020 at 09:43:47 LT (*a*); a sunspot subimage in the focal plane of the Shack—Hartmann wavefront sensor (*b*)

$$C_{sx} = \left\langle \delta x_1(s,0) \delta x_2(s,\alpha) \right\rangle = \sum_{n=1}^{N} c_n(h_n) F_x(s,\alpha,h_n), \tag{1}$$

$$C_{sy} = \left\langle \delta y_1(s,0) \delta y_2(s,\alpha) \right\rangle = \sum_{n=1}^{N} c_n(h_n) F_y(s,\alpha,h_n), \tag{2}$$

where s is the distance from the reference subaperture multiple of 6 cm; α is the angle between sunspot centers; h_n is the height of the turbulent layer n; δx_1 and δy_1 are differential center-of-gravity shifts in the first sunspot along conventionally chosen X- and Y-axes; δx_2 and δy_2 are the same for the second sunspot. $F_x(s, \alpha, h_n)$ and $F_y(s, \alpha, h_n)$ are expansion functions depending on the number of subapertures in the wavefront sensor, the angular distance between sunspot centers, and height. Expressions (1) and (2) are linear expansions of cross-correlation functions C_{sx} and C_{sy} in dimensionless structure characteristics of turbulence c_n taken with weights $F_x(s, \alpha, h_n)$ or $F_y(s, \alpha, h_n)$ for the x and y components of differential subimage shifts.
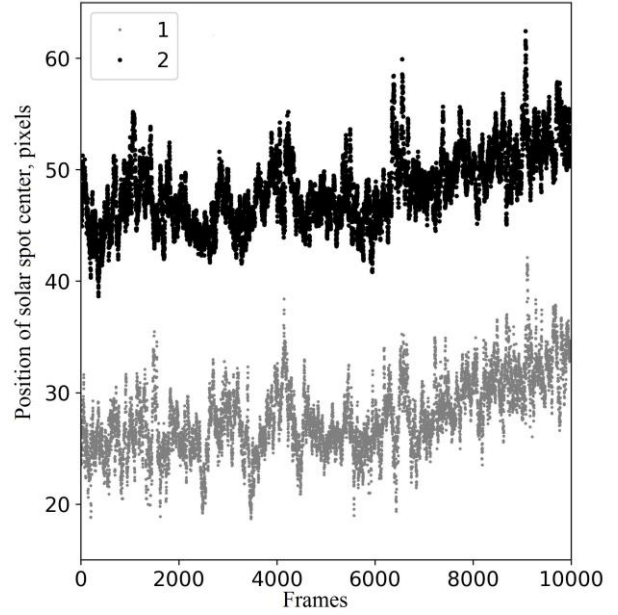
Figure 4 shows time realizations of dimensionless turbulence energy in different atmospheric layers, estimated from LSVT observations. Along the X-axis are eleven 26 s time intervals N_l; along the Y-axis, values of dimensionless turbulence energy I_f. When determining I_f, we assumed that the average maximum variance, calculated from integral differential center-of-gravity shifts in the subimages of the first sunspot, is equal to 1 (line 4). Turbulence energy in each layer was normalized to the total energy, taking into account that the sum of energies over the layers should be equal to the energy calculated from the integral differential center-of-gravity shifts in the subimages of the first sunspot (energy of the optically active layer of the atmosphere from the telescope aperture to a height of 20 km). In other words, we assumed that the sum of structure constants of air refractive index fluctuations is equal to the sum of c_n values over the layers δh_n thick:

$$\sum_{n=1}^{N} C_n^2(h_n)\delta h_n = a_t \sum_{n=1}^{N} D_{\text{eff}}^{1/3}(h_n)c_n(h_n)\delta h_n, \qquad (6)$$

where a_t is the coefficient of proportionality.

Analysis of Figure 4 shows that over the period of interest the amplitude of differential subimage motion (integral over the line of sight of the telescope) decreased on the average, and the image quality improved. Table lists average estimates of the contribution of atmospheric layer turbulence to the total intensity for a series of LSVT measurements.

With height, the contribution of the turbulent layers to the turbulence energy estimated from the integral motion decreases. We can assume that the optical turbulence concentrated in the atmospheric layer ~1.7 km thick is ~43 % of the integral optical turbulence intensity.
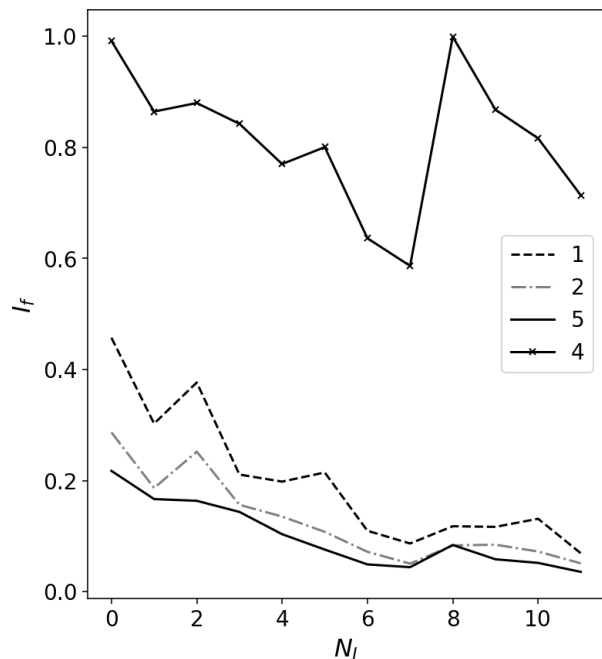

Figure 4. Time realizations of dimensionless turbulence energy estimated from LSVT observations: 1 — layer at a height of 564 m, 2 — 1129 m, 3 — 1693 m, 4 — variations in the dimensionless turbulence energy integral over the line of sight

In practice, this means that the observed low image quality is mainly due to optical turbulence in the lower atmospheric layers (according to estimated turbulence formed in a layer to 3.5 km).

Contribution to the total turbulence intensity of different atmospheric layers

Distance, km	Layer thickness, km	Contribution to total turbulence intensity, %
0–1.1	0–0.6	19.9
1.1–2.2	0.6–1.1	12.8
2.2–3.2	1.1–1.7	9.9
0–3.2	0–1.7	42.6

DISCUSSION

We have presented the results of studies of wavefront distortions along the LSVT line of sight at different heights in the atmosphere. Optical turbulence characteristics at different heights were determined by analyzing spatial cross-correlation functions of differential center-of-gravity shifts in sunspot subimages on spaced subapertures of the Shack–Hartmann wavefront sensor.

The use of the differential center-of-gravity shifts in subimages for the calculations made it possible to avoid the influence of mechanical vibrations of LSVT. We have drawn the following conclusions.

1. From measurements made with the Shack–Hartmann wavefront sensor at LSVT, we have determined optical turbulence characteristics for the atmospheric layers 0–0.6, 0.6–1.1, 1.1–1.7, and 0–1.7 km. The contribution of optical turbulence in an atmospheric layer ~1.7 km thick to the amplitude of wavefront distortions at the telescope aperture is shown to be ~43 %.

2. The high percentage of the contribution of the lower atmospheric layers at the location of LSVT indicates the presence of time intervals with low energy of optical turbulence in upper atmospheric layers. To achieve acceptable Strehl parameter, we assume that under conditions of such an optical turbulence energy distribution with height it can be effective to use a multicascade AO system with optical conjugation of deformable mirrors with turbulent layers. Heights of the conjugation and parameters of the deformable mirrors should be refined taking into account estimated phase dispersion balance.

We have employed the S-DIMM+ method adapted to work on two sunspots. A necessary condition for this method is the presence of two sunspots within a field of view limited to a few arcmin. Sunspots are associated with emergence of strong magnetic fields from the convective zone of the Sun. Due to emergence of magnetic tubes, sunspots usually form in groups and are often located relatively close to each other. Current views about the emergence of magnetic fields explain well the observed properties of sunspots such as bipolarity, their orientation, polarity inversion with time and latitude, the slope angle of group of sunspots and their position at low latitudes.

The characteristic size of sunspots varies from 5 to 50 Mm, and their lifetime ranges from several hours to several months. The spatial distribution of sunspots over

the Sun and their number primarily depend on the solar cycle phase. The cyclicity of sunspot formation is usually represented as the Maunder butterfly diagram [Arlt et al., 2020]. Analysis of the Maunder butterfly diagram makes it possible to determine the spatial localization and number of sunspots. In this case, individual sunspots and sunspot groups are observed even during solar minima. Turbulence monitoring using two sunspots can be performed routinely in the AO system, excluding periods of solar minimum when only individual observations are possible. In the future, the method can be adapted to a large number of sunspots, providing additional nodes in the reconstruction of vertical profiles of optical turbulence. Developing and applying optical turbulence profiling methods, obtaining statistically valid profiles of optical turbulence characteristics for different levels of solar image quality are the steps necessary to devise an AO system for a solar telescope, which can correct images in a field of view above 1–3 arcsec. The development of an AO system for systematic observations under conditions of mean turbulence intensity should be based on the cascade principle and include a tip/tilt corrector and several deformable mirrors, including those coupled to the telescope aperture and providing correction of significant amplitudes of high-order aberrations. This approach is confirmed by the results of testing of the adaptive LSVT system with one deformable mirror providing incomplete (partial) correction of wavefront aberrations [Lukin et al., 2020]. Our findings can be useful for commissioning the adaptive optics system of the Large Solar Telescope LST-3 [Grigoryev et al., 2020].

REFERENCES

Arlt R., Vaquero J.M. Historical sunspot records. *Living Rev. Solar Phys*. 2020, vol. 17, iss. 1, article id. 1. DOI: 10.1007/s41116-020-0023-y.

Banakh V.A., Smalikho I.N., Falits A.V. Estimation of the height of the turbulent mixing layer from data of Doppler lidar measurements using conical scanning by a probe beam. *Atmospheric Measurement Techniques*. 2021, vol. 14, iss. 2, pp. 1511–1524. DOI: 10.5194/amt-14-1511-2021.

Bolbasova L.A., Lukin V.P. Atmospheric research for adaptive optics problem. *Optika atmosfery i okeana.* [Atmospheric and Oceanic Optics J.]. 2021, vol. 34, no. 4, pp. 254–271. DOI: 10.15372/AOO20210403. (In Russian).

Botygina N.N., Emaleev O.N., Konyaev P.A., Kopylov E.A., Lukin V.P. Development of components for adaptive optics systems for solar telescopes. *Atmospheric and Oceanic Optics*. 2018, vol. 31, pp. 216–223. DOI: 10.1134/S1024856018020057.

Grigoryev V.M., Demidov M.L., Kolobov D.Yu., Pulyaev V.A., Skomorovsky V.I., Chuprakov S.A. AMOS team Project of the Large Solar Telescope with mirror 3 m in diameter. *J. Solar-Terr. Phys*. 2020, vol. 6, iss. 2, pp. 14–29. DOI: 10.12737/stp-62202002.

Kamardin A.P., Odintsov S.L. Height profiles of the structure characteristic of air temperature in the atmospheric boundary layer from sodar measurements. *Atmospheric and Oceanic Optics*. 2017, vol. 30, iss. 1, pp. 33–38. DOI: 10.1134/S1024856017010079.

Kazakov D.V., Lavrinov V.V., Lavrinova L.N. Results of numerical testing of algorithms for centering of focal spots in a Shack-Hartmann wavefront sensor. *Proc. SPIE. 24th International Symposium on Atmospheric and Ocean Optics: Atmospheric Physics*; Tomsk. 2018, vol. 10833, 108332D. DOI: 10.1117/12.2504557.

Kleimenov V.V., Vozmishchev I.Yu., Novikova E.V. Application limitations of a laser guide star in adaptive optoelectronic systems caused by its jitter in the atmosphere. *J. Optical Technology*. 2021, vol. 88, iss. 10, pp. 569–573. DOI: 10.1364/JOT.88.000569.

Kornilov V., Vozyakova O., Safonov B., Shatsky N., Ilyasov S., Tillaev Y., Ibragimov M., Egamberdiev S. Measurement of optical turbulence in free atmosphere above Mt. Maidanak in 2005–2007. *Astron. Lett*. 2009, vol. 35, no. 8, pp. 547–554. DOI: 10.1134/S1063773709080040.

Kovadlo P.G., Lukin V.P., Shikhovtsev A.Yu. development of the model of turbulent atmosphere at the Large Solar Vacuum Telescope site as applied to image adaptation. *Atmospheric and Oceanic Optics*. 2019, vol. 32, pp. 202–206. DOI: 10.1134/S1024856019020076.

Lavrinov V.V., Lavrinova L.N. Reconstruction of wavefront distorted by atmospheric turbulence using a Shack—Hartman sensor. *Computer Optics*. 2019, vol. 43, iss. 4, pp. 586–595. DOI: 10.18287/2412-6179-2019-43-4-586-595.

Lukin V.P., Botygina N.N., Antoshkin L.V., Borzilov A.G., Emaleev O.N., Konyaev P.A., Kovadlo P.G., Kolobov D.Yu., Selin A.A., Soin E.L., Shikhovtsev A.Y., Chuprakov S.A. Multi-Cascade Image Correction System for the Large Solar Vacuum Telescope. *Atmospheric and Oceanic Optics*. 2019, vol. 32, iss. 5, pp. 597–606. DOI: 10.1134/S1024856019050117.

Lukin V.P., Antoshkin L.V., Bol'basova L.A., Botygina N.N., Emaleev O.N., Kanev F.Yu., Konyaev P.A., Kopylov E.A., Lavrinov V.V., Lavrinova L.N., Makenova N.A., Nosov V.V., Nosov E.V., Torgaev A.V. The history of the development and genesis of works on adaptive optics in the Institute of atmospheric optics. *Atmospheric and Oceanic Optics*. 2020, vol. 33, iss. 1, pp. 85–103. DOI: 10.1134/S1024856020010078.

Marco de la Rosa J., Montoya L., Collados M., Montilla I., Vega Reyes N. Daytime turbulence profiling for EST and its impact in the solar MCAO system design. *Proc. SPIE. Adaptive optics systems V*; Edinburgh, United Kingdom. 2016, vol. 9909, 99096X. DOI: 10.1117/12.2229471.

Nosov V.V., Lukin V.P., Nosov E.A., Torgaev A.V. Method for atmospheric turbulence profile measurement from observation of laser guide stars. *Atmospheric and Oceanic Optics*. 2017, vol. 30, iss. 2, pp. 176–183. DOI: 10.1134/S1024856017020099.

Odintsov S.L., Gladkikh V.A., Kamardin A.P., Nevzorova I.V. Determination of the structural characteristic of the refractive index of optical waves in the atmospheric boundary layer with remote acoustic sounding facilities. *Atmosphere*. 2019, vol. 10. iss. 11, p. 711. DOI: 10.3390/atmos10110711.

Rasouli S., Rajabi Y. Investigation of the inhomogeneity of atmospheric turbulence at day and night times. *Optics and Laser Technology*. 2016, vol. 77, pp. 40–50. DOI: 10.1016/j.optlastec.2015.08.017.

Rasouli S., Ramaprakash A.N., Das H.K., Rajarshi C.V., Rajabi Y., Dashti M. Two channel wavefront sensor arrangement employing Moiré deflectometry. *Proc. SPIE. Optics in Atmospheric Propagation and Adaptive Systems XII*; Berlin, Germany, 2009, vol. 7476, 74760K. DOI: 10.1117/12.829962.

Potekaev A., Shamanaeva L., Kulagina V. Spatiotemporal dynamics of the kinetic energy in the Atmospheric Boundary layer from minisodar measurements. *Atmosphere.* 2021, vol. 12, iss. 4, p. 421. DOI: 10.3390/atmos12040421.

Shikhovtsev A.Y., Chuprakov S.A., Kovadlo P.G. Sensor to register the optical distortions in the wide field of view of solar telescope. *Proc. SPIE. XIV International Conference on Pulsed Lasers and Laser Applications*; Tomsk, Russia. 2020, vol. 11322, id. 113220B. DOI: 10.1117/12.2553045.

Shikhovtsev A.Yu., Lukin V.P., Kovadlo P.G. The development of the adaptive optics systems for the ground-based solar telescopes. *Optika atmosfery i okeana.* [Atmospheric and Oceanic Optics J.]. 2021a, vol. 34, no. 5, pp. 385–392. DOI: 10.15372/AOO20210512. (In Russian).

Shikhovtsev A.Y., Kovadlo P.G., Kiselev A.V., Kolobov D.Y., Lukin V.P., Russkikh I.V., Shikhovtsev M.Y. Modified method to detect the turbulent layers in the atmospheric boundary layer for the Large Solar Vacuum Telescope. *Atmosphere.* 2021b, vol. 12, p. 159. DOI: 10.3390/atmos12020159.

Song T., Cai Z., Liu Y., Zhao M., Fang Y., Zhang X., Wang J., Li X., Song Q., Du Z. Daytime optical turbulence profiling with a profiler of the differential solar limb. *Monthly Notices of the Royal Astronomical Society*. 2020, vol. 499, iss. 2, pp. 1909–1917. DOI: 10.1093/mnras/staa2729.

Wang Z., Zhang L., Kong L., Bao H., Guo Y., Rao X., Zhong L., Zhu L., Rao C. A modified S-DIMM+: Applying additional height grids for characterizing daytime seeing profiles. *Monthly Notices of the Royal Astronomical Society.* 2018, vol. 478, iss. 2, pp. 1459–1467. DOI: 10.1093/mnras/sty1097.

How to cite this article
Shikhovtsev A.Yu., Kiselev A.V., Kovadlo P.G., Kolobov D.Yu., Russkikh I.V., Tomin V.E. Turbulent parameters at different heights in the atmosphere. Shack—Hartmann wavefront sensor data. *Solar-Terrestrial Physics*. 2022. Vol. 8. Iss. 2. P. 20–25. DOI: 10.12737/stp-82202203.